



http://pubs.acs.org/journal/acsodf Article

Large Non-planar Conjugated Molecule with Strong Intermolecular Interactions Achieved with Homoleptic Zn(II) Complex of Di(5quinolylethynyl)-tetraphenylazadipyrromethene

Chenwei Lu, Chunlai Wang, Jayvic C. Jimenez, Arnold L. Rheingold, and Genevieve Sauvé*



Cite This: ACS Omega 2020, 5, 31467-31472



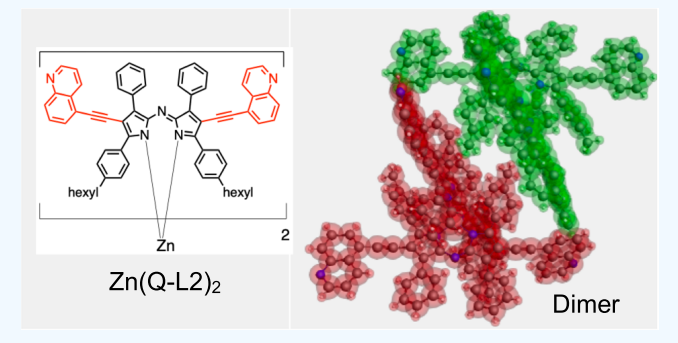
ACCESS I

III Metrics & More

Article Recommendations

s Supporting Information

ABSTRACT: Zinc(II) complexes of tetraphenylazadipyrromethenes are potential non-planar n-type conjugated materials. To tune the properties, we installed 5-quinolylethynyl groups at the pyrrolic positions. Compared to the complex with 1-napthylethynyl, we found evidence for stronger intermolecular interactions in the new complex, including much higher overlap integrals in crystals. X-ray analysis revealed unconventional C-H···N hydrogen bonding between two quinolyls of neighboring molecules, pointing to a new strategy for the development of non-planar molecular semiconductors with stronger intermolecular interactions.



1. INTRODUCTION

 π -Conjugated systems have attracted much attention due to their remarkable optical and electronic properties.^{1,2} Optimization of charge transport properties is usually done by designing planar conjugated systems to facilitate charge transport along the conjugated backbone and strong intermolecular π – π stacking between planar backbones to facilitate intermolecular charge transport.^{3–7} This strategy has been successful for applications using field-effect transistor device geometries but has fallen short for applications using diode-type devices, such as organic photovoltaics (OPVs). In solution-processable OPVs, the active layer consists of a p-type material that is often a conjugated polymer and an n-type material that is often a fullerene derivative or, more recently, a conjugated molecule.^{8–10} In these types of blends, a large planar *n*-type material unfavorably phase separates from the conjugated polymer on a large scale. ^{11,12} Instead, either a nonplanar geometry or a planar geometry with bulky side chains has been used as a design strategy to simultaneously optimize co-planarity and intermolecular interactions while toning down the propensity for self-aggregation. 13-16

We have discovered that zinc complexes of tetraphenylazadipyrromethenes (ADP, Figure 1) are promising candidates for an n-type material due to their non-planarity, rigid conjugation, and high absorptivity in the visible range.¹⁷ The most promising derivative incorporates 1-naphthylethynyl groups at the pyrrolic positions, Zn(L2)2, which has high absorption between 600 and 800 nm, isotropic charge transport, and a high PCE of 5.5% when blended with the most studied and cheapest conjugated polymer donor, poly(3-hexylthiophene) (P3HT).^{20–23} Moreover, its facile synthesis

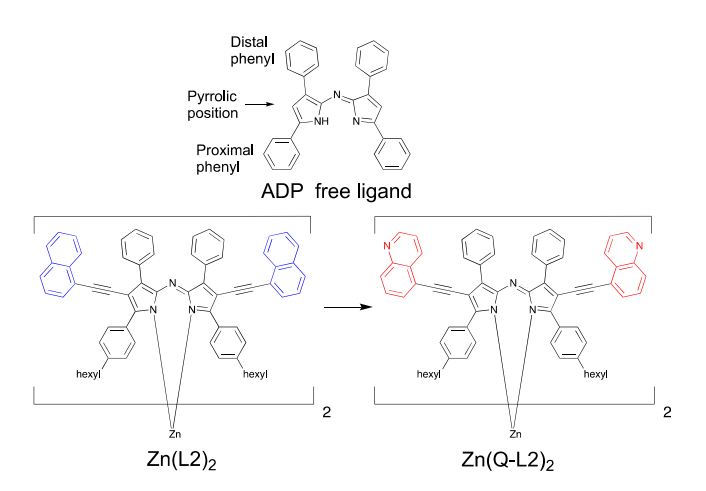


Figure 1. Chemical structure of ADP and zinc(II) complexes.

from inexpensive starting materials and simple purification makes it promising for practical applications. 20,24 To further tune properties, we replaced the naphthyl groups with quinolyl, see Figure 1. The estimated HOMO energy levels of the new complex were slightly lowered due to the more electron-poor quinolyl groups. Interestingly, analysis of the crystal structure

Received: October 23, 2020 Accepted: November 13, 2020 Published: November 25, 2020





revealed stronger intermolecular interactions with unconventional C-H···N hydrogen bonding that is not present in Zn(L2)₂. This discovery points to a new strategy for developing materials with stronger intermolecular interactions.

2. RESULTS AND DISCUSSION

The synthesis of $Zn(Q-L2)_2$ is depicted in Scheme 1. 5-Ethynylquinoline **b** was obtained by Sonogashira coupling of 5-

Scheme 1. Synthesis of Zn(Q-L2)2

"(i) Toluene, triethylamine, CuI, and Pd(PPh₃)₂Cl₂, 50 °C, 16 h; (ii) methanol/Et₂O, K₂CO₃, 25 °C, 45 min; (iii) THF, LDA, and tributyltin chloride; (iv) Pd(PPh₃)₄ and xylenes, 120 °C, 3 h; (v) THF and NaH, 40 °C, 1 h, followed by CH₂Cl₂ and ZnCl₂/MeOH, 25 °C, overnight.

bromoquinoline with ethynyltrimethylsilane followed by deprotection using K₂CO₃ as the base. Tributyl tin compound c was synthesized from b by deprotonation of the ethynyl using lithium diisopropylamide (LDA) and tributyltin chloride. Note that it was necessary to use LDA rather than n-butyllithium to obtain pure c in good yield because n-butyllithium can attack at the quinoline's 2-position.²⁵ The ligand Q-L2 was obtained by Stille coupling of tributyl tin compound c with the iodinated precursor pr-hexylADPI₂ in 80% yield. Due to its low solubility in common organic solvents, the identity of the ligand was only confirmed by MALDI-TOF MS. The synthesis of the zinc complex was successfully performed following the published procedure for Zn(L2)₂, ²⁰ with a 65% yield. The zinc complex is soluble in common organic solvents such as chloroform, THF, and DCM. The identity and purity of Zn(Q-L2), were confirmed by NMR, MALDI-TOF-MS, and elemental analysis.

Thermal gravimetric analysis revealed that the complex is stable with a 5% weight loss at 421 °C (Figure S8). Crystals grown by hexane/DCM liquid diffusion were analyzed by differential scanning calorimetry (Figure S9 and Table S1). The first heating cycle shows a small endothermic peak at 205 °C, assigned to side chain movement, followed by a sharp endothermic peak at 248 °C, corresponding to the crystal melting with a heat of fusion of 37 J/g. The melting temperature of Zn(Q-L2)₂ is 19 °C higher than that of Zn(L2)₂, pointing to stronger intermolecular interactions in Zn(Q-L2)₂, suggesting lower crystallinity in the Zn(Q-L2)₂ crystals. The first cooling cycle and all subsequent heating and cooling cycles were featureless, consistent with the complex becoming amorphous after melting.

The UV—vis absorption spectra of $Zn(Q-L2)_2$ are shown in Figure 2, and the optical properties are summarized in Table 1. The data for $Zn(L2)_2$ were included for comparison. Both complexes have similar absorption spectra. In solution, the λ_{max}

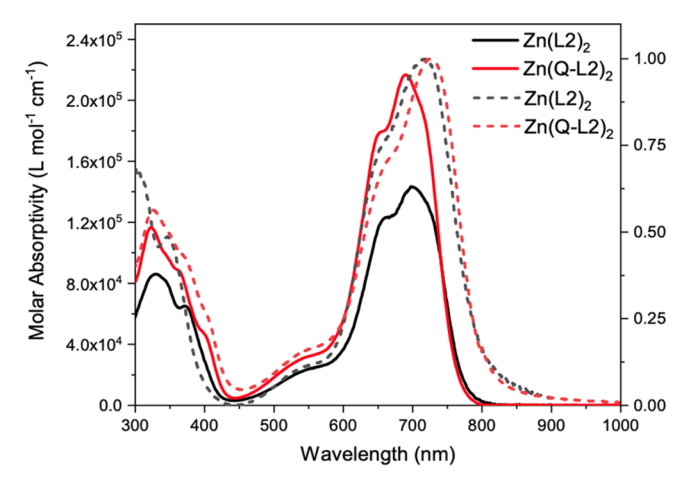


Figure 2. UV-vis absorption spectra in solution (full line) and in film (dashed line) of $Zn(Q-L2)_2$ and $Zn(L2)_2$.

Table 1. Summary of Optical Properties of $Zn(L2)_2$ and $Zn(Q-L2)_2$

compound	solution λ_{max} (nm) $(\varepsilon, \times 10^3 \text{ M}^{-1} \text{ cm}^{-1})$	film λ_{max} (nm) (α , ×10 ⁵ cm ⁻¹)	$\begin{array}{c} \text{optical} \\ \text{gap } E_{\text{g}} \\ \text{(eV)} \end{array}$	$\Delta \lambda_{max}$ (nm) upon film formation
$Zn(L2)_2^a$	330 (86), 372 (65), 664 (123), 700 (143)	727 (2.13)	1.54	27
$Zn(Q-L2)_2$	324 (92), 363 (89), 650 (140), 690 (217)	726 (0.99)	1.56	36

^aData obtained from ref 20.

of $Zn(Q-L2)_2$ is 690 nm, blueshifted by ~10 nm compared to $Zn(L2)_2$, and has a higher absorptivity coefficient of 2.17×10^5 M⁻¹ cm⁻¹, compared to 1.43×10^5 M⁻¹ cm⁻¹ for $Zn(L2)_2$. In films, the λ_{max} for $Zn(Q-L2)_2$ is 726 nm, similar to $Zn(L2)_2$ at 727 nm. This corresponds to a redshift of 36 and 27 nm upon film formation of $Zn(Q-L2)_2$ and $Zn(L2)_2$, respectively, suggesting stronger intermolecular interactions in $Zn(Q-L2)_2$ films. The optical gap of $Zn(Q-L2)_2$, taken as the film absorption onset, is 1.56 eV, similar to $Zn(L2)_2$.

The cyclic voltammograms (CVs) of the zinc complexes in dichloromethane are shown in Figure 3, and the electrochemical properties are summarized in Table 2. The CV of

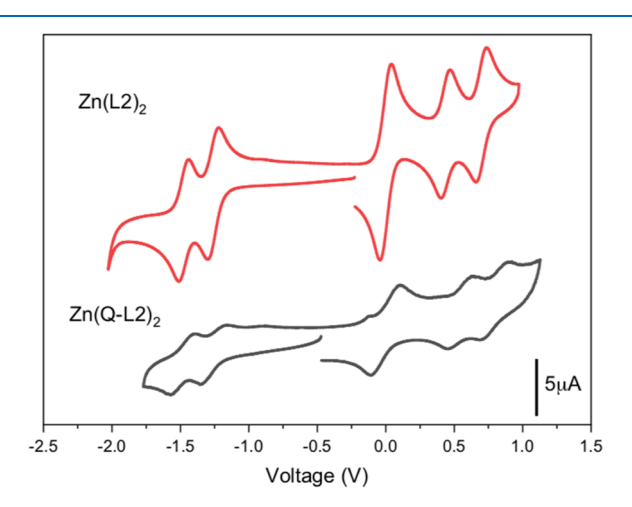


Figure 3. Cyclic voltammograms of Zn complexes in 0.1 M TBAPF $_6$ dichloromethane solution with Fc/Fc $^+$ as an internal standard.

Table 2. Electrochemical Properties of Zinc Complexes in Dichloromethane^a

compound	$E_{1/2}$ ox. (V)	E_{onset} first ox. (V)	$E_{1/2}$ red. (V)	$E_{\rm onset}$ first red. (V)	$HOMO/LUMO^b$ (eV)	$E_{\rm gap}~({\rm eV})$
$Zn(L2)_2^a$	0.44, 0.71	0.37	-1.26, -1.48	-1.18	-5.17/-3.62	1.56
$Zn(Q-L2)_2$	0.55, 0.80	0.49	-1.27, -1.49	-1.17	-5.29/-3.63	1.66

[&]quot;Data obtained from ref 21. Estimated HOMO/LUMO energy levels obtained from the $E_{\rm onset}$ and using the value of -4.8 eV for Fc/Fc⁺ versus vacuum.

Zn(Q-L2) is similar to $Zn(L2)_2$ with two reversible reductions waves and two reversible oxidation waves, typical for homoleptic zinc complexes of ADP. Replacing naphthyl with quinolyl increased the oxidation potentials by 0.1 V but did not impact the reduction potentials. The highest occupied molecular orbital (HOMO) and the lowest unoccupied molecular orbital (LUMO) were estimated using the first oxidation and first reduction onsets, respectively. The estimated HOMO and LUMO energy levels are -5.29 and -3.63 eV, respectively.

Crystals of $Zn(Q-L2)_2$ were analyzed by single-crystal X-ray diffraction, and the thermal ellipsoid plot is shown in Figure 4A. The complex has a distorted tetrahedral structure with a

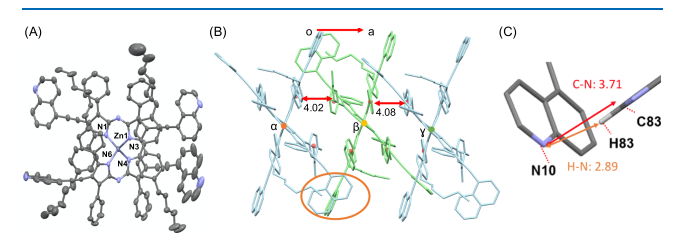


Figure 4. (A) Thermal ellipsoid plot of $Zn(Q-L2)_2$ (50% probability level). The hydrogen atoms were omitted for clarity. (B) Stick model for dimers of $Zn(Q-L2)_2$, showing intermolecular $\pi-\pi$ interactions in the oa direction, each complex is labeled for calculation discussion. (C) Expanded graph of orange circle in (B) at a different angle, showing intermolecular hydrogen bonding between quinolyl groups. (H83-N10: 2.89 Å, C83-N10: 3.71 Å).

dihedral angle of 71.3° and a $\pi-\pi$ stacking distance between the proximal phenyl of one ligand and pyrrole of the other ligand of 3.54 Å. For comparison, the dihedral angle and intramolecular distance for $\text{Zn}(\text{L2})_2$ is 72.2° and 3.73 Å, respectively. Interestingly, three of the quinolyl groups lie in the same plane as the ADP core, but one is at a dihedral angle of 89.76° from the ADP core (Figure S12E). This twist is likely driven by intermolecular interactions in the crystal.

To investigate the intermolecular interactions, we looked at the crystal packing. The unit cell consists of two molecules, which we label α and β in Figure 4B. In the unit cell, we observe parallel-displaced $\pi-\pi$ interactions between proximal and distal phenyl groups with a distance of 4.02 Å (see Table 3). This is in contrast to $\text{Zn}(\text{L2})_2$, whose intermolecular $\pi-\pi$ interactions are T-shaped and have larger distances. Interest-

Table 3. Summary of Intermolecular Interactions in Zn(Q-L2)₂ Crystals in the oa Crystallographic Direction^a

pair	type of interaction	D (Å)	Ve- (meV)	Vh+ (meV)
α - β (unit cell)	proximal-distal π – π (P), hydrogen bonding	4.02, 3.71	12	5.9
β - γ (cross cell, <i>a</i> axis)	proximal-distal π – π (P)	4.08	6.1	4.55

^aP is parallel, and D is the intermolecular distance.

ingly, the pyrrolic quinolyl groups have intermolecular interactions between the nitrogen atom of one quinolyl (strong hydrogen-bond acceptor) and the α hydrogen of another quinolyl (weak hydrogen-bond donor), with a N···C distance of 3.71 Å, Figure 4C. Unconventional C–H···N hydrogen bonds have been observed in peptides and are considered very weak. Across the unit cell in the oa crystallographic direction (between β and γ molecules in Figure 4B), we observe parallel-type π - π interactions between proximal and distal phenyl groups with a distance of 4.08 Å but no hydrogen bonding. Pairs in the ob and oc directions also do not show any hydrogen bonding.

The strength of the noncovalent hydrogen bonding interaction between the two quinolyl groups was estimated computationally by performing an energy decomposition analysis (EDA). This was done using a dispersion-corrected density functional theory (DFT) (BLYP functional with D3(BJ) correction and TZ2P basis set) in the Amsterdam density functional (ADF) code, which has been shown to be applicable for noncovalent interactions, including H bonding and π - π stacking. The analysis revealed an intermolecular interaction energy of -4.1 kcal/mol between the two quinolyl groups, with a low electrostatic contribution of -1.4 kcal/mol (Table S3). This confirms that the hydrogen bonding interaction is weak. S5-37 Because the hydrogen bond interaction is similar in strengths to π - π interactions, we surmise that it contributes to guide crystal packing in Zn(Q-L2)₂.

To quantify intermolecular interactions, the charge transfer integrals V were computed between two molecules from the crystal structure using DFT and single-point calculations in the ADF code. 32,33,38-40 To simplify the calculations, the hexylsolubilizing groups were replaced with methyls. The calculated electron and hole transfer integrals are included in Table 3, and the results for other pairs in the crystal with non-zero transfer integrals are given in Table S4. The transfer integrals calculated for the unit cell were the highest at 12 and 5.9 meV for the electron and hole transfer integrals, respectively. The transfer integrals across the unit cell for Zn(Q-L2)2 in the oa direction $(\beta-\gamma)$ were lower than in the unit cell at 6.1 and 4.55 meV for the electron and hole transfer integrals, respectively. These results are consistent with H bonding contributing to increase the charge transfer integral in the unit cell of $Zn(Q-L2)_2$. We also calculated smaller but non-zero transfer integrals across cells in the ob and oc directions (Table S4), indicating that charges can transfer in 3D, though it is the strongest in the general oa direction.

The transfer integrals for the unit cell of $Zn(Q-L2)_2$ are about four times higher than the values calculated for $Zn(L2)_2$ (Table S4). The transfer integrals in the oa direction are also significantly larger for $Zn(Q-L2)_2$ than for $Zn(L2)_2$. These results are consistent with stronger intermolecular interactions in $Zn(Q-L2)_2$. Considering that charge transfer rates are proportional to V^2 and that charge transfer rates are directly proportional to charge carrier mobility, these results imply that

 $Zn(Q-L2)_2$ has the potential to have higher charge carrier mobilities than $Zn(L2)_2$.

3. CONCLUSIONS

In summary, a new zinc complex of ADP incorporating 5quinolylethynyl groups at the pyrrolic positions was successfully synthesized and characterized. Zn(Q-L2)2 has higher oxidation potentials but similar reduction potentials than Zn(L2)₂. Compared to the Zn(L2)₂, the UV-vis absorption spectra slightly blueshift in solution but are similar in films, resulting in a larger redshift upon film formation for Zn(Q-L2)2. This points to increased intermolecular interactions, which is also supported by the higher melting point and the higher estimated overlap integrals in dimers obtained from the crystal structures. Contributing to the morphology of Zn(Q-L2)₂ in crystals is weak hydrogen bonding between quinolyl groups of two adjacent complexes. This work suggests that intermolecular interactions can be enhanced using weak hydrogen bonding, opening new opportunities for the development of non-planar organic semiconductors.

4. EXPERIMENTAL SECTION

- 4.1. Materials. 4-Hexylacetophenone (TCI America), benzaldehyde (Aldrich), lithium diisopropylamide solution (Aldrich), tributyltin chloride (Fisher), 5-bromoquinoline (Aldrich), tetrakis(triphenylphosphine)palladium(0) (Aldrich), bis(triphenylphosphine)platinum(II) chloride (Aldrich), copper(I) iodide (TCI America), N-iodosuccinimide, (abbreviated as NIS, Aldrich), nitromethane (Aldrich), ferrocene (Aldrich), diethylamine, anhydrous dichloromethane (Aldrich), zinc(II) chloride (Aldrich diethylamine (Aldrich), anhydrous dichloromethane (Aldrich), zinc(II) chloride (Aldrich), trimethylamine (Aldrich), acetic acid (Fisher), and chloroform (Aldrich) were used as received. Xylenes and tetrahydrofuran (THF) were distilled over sodium and stored in a refrigerator before use. All other chemicals were purchased from either Sigma Aldrich or Fisher Scientific and used as received.
- 4.2. 5-((Trimethylsilyl)ethynyl)quinoline (a). A 250 mL oven-dried Schlenk flask was charged with 5-bromoquinoline (1.5 g, 7.2 mmol), ethynyltrimethylsilane (0.99 g, 10 mmol), Pd(PPh₃)₂Cl₂ (0.50 g, 0.72 mmol), CuI (0.27 g, 1.4 mmol), distilled triethylamine (25 mL), and anhydrous toluene (80 mL) under nitrogen. The flask was then placed in a pre-heated oil bath at 50 °C. The reaction mixture turned brown upon heating. The mixture was then stirred at 50 °C for 16 h. After cooling to room temperature, the reaction mixture was filtered through a Celite plug. The filtrate was collected, and the volatile species were removed by rotary evaporation. The remaining brown oil was purified by gradient silica column chromatography (1:5-1:3 AcOEt/hexanes) to give a (1.37 g, 84.3%) as a brown liquid. ¹H NMR (500 MHz, chloroform-d) δ 8.95 (dd, J = 3.6, 1.8 Hz, 1H), 8.67–8.60 (m, 1H), 8.14– 8.06 (m, 1H), 7.75 (dq, J = 7.1, 1.3 Hz, 1H), 7.65 (dtt, J = 9.5, 4.0, 2.5 Hz, 1H), 7.57-7.43 (m, 1H), 0.33 (s, 9H).
- **4.3. 5-Ethynylquinoline (b).** A 250 mL round bottle flask was treated with a (1.33 g, 4.44 mmol), $\rm Et_2O$ (50 mL), methanol (15 mL), and potassium carbonate (3.68 g, 26.6 mmol). The mixture was stirred vigorously at room temperature. After 45 min, the reaction was quenched by pouring into 200 mL water. The layers were separated, and the aqueous layer was extracted with $\rm Et_2O$ (3 × 40 mL). The combined

- organic layer was washed with water (3 × 50 mL) and brine (2 × 50 mL) and then dried over MgSO₄. The solvent was removed by rotary evaporation. The remaining brown crystalline solid was deposited on a silica gel and purified by silica flash column chromatography (1:3 AcOEt/hexanes) to give **b** (0.69 g, 80%) as a white crystalline solid. ¹H NMR (500 MHz, chloroform-d) δ 8.96 (dd, J = 4.3, 1.7 Hz, 1H), 8.69–8.63 (m, 1H), 8.13 (d, J = 8.5 Hz, 1H), 7.79 (d, J = 7.1 Hz, 1H), 7.67 (dd, J = 8.5, 7.2 Hz, 1H), 7.50 (dd, J = 8.4, 4.2 Hz, 1H), 3.49 (s, 1H).
- 4.4. 5-((Tributylstannyl)ethynyl)quinoline (c). An oven-dried 100 mL Schlenk flask was charged with b (0.50 g, 3.3 mmol) and anhydrous THF (60 mL) under nitrogen. The solution was cooled to -78 °C via an acetone/dry ice bath and stirred 15 min before the dropwise addition of LDA solution (2.0 M in THF/heptane/ethylbenzene, 1.80 mL, 3.59 mmol). The solution turned yellow upon the completion of addition. The mixture was then stirred for an additional 15 min before the dropwise addition of tributyltin chloride (1.17 g, 3.59 mmol). Immediately upon the complete addition of tributyltin chloride, the mixture was warmed to room temperature and stirred for 30 min. THF and hexanes were removed by rotary evaporation. The residue in the flask was then filtered through a filter paper and washed with hexanes, and the filtrate was collected. Hexanes were then removed by rotary evaporation to give c as a yellow oil (1.3 g, 90%). ¹H NMR (500 MHz, chloroform-d) δ 8.93 (dd, I = 4.1, 1.8 Hz, 1H), 8.70 (d, J = 8.2 Hz, 1H), 8.04 (d, J = 8.4 Hz, 1H), 7.72 (d, J = 7.1 Hz, 1H), 7.66 - 7.59 (m, 1H), 7.46 (dd, J = 8.4, 4.2)Hz, 1H), 1.73-1.62 (m, 6H), 1.41 (q, J = 7.4 Hz, 6H), 1.13(dd, J = 9.1, 7.0 Hz, 6H), 0.94 (t, J = 7.4 Hz, 9H).
- **4.5. Q-L2.** A 100 mL oven-dried Schlenk flask was charged with pr-hexylADPI₂ (0.30 g, 0.34 mmol), 20 c (0.34 g, 0.76 mmol), Pd(PPh₃)₄ (40 mg, 0.03 mmol), and degassed xylene (50 mL) under nitrogen. The flask was then placed in a preheated oil bath at 120 °C. Upon heating, the reaction mixture turned blue, and blue solids precipitated out. The mixture was stirred at 120 °C for 3 h. After cooling to room temperature, the reaction mixture was poured into MeOH (200 mL). The resulting mixture was filtered through a filter paper, and the solid was washed with MeOH (50 mL) and hexanes (100 mL) to give Q-L2 as a blue solid (0.25 g, 80%). MALDI-TOF-MS m/z calcd. for $C_{66}H_{57}N_5$, 919.46; found, 919.53.
- **4.6.** Zn(Q-L2)₂. A 100 mL oven-dried Schlenk flask was charged with Q-L2 (0.14 g, 0.15 mmol), NaH (8 mg, 0.3 mmol), and THF (8 mL) under nitrogen. The reaction mixture was stirred at 40 °C for 1 h. After cooling the mixture to room temperature, anhydrous dichloromethane (50 mL) was added into the mixture via a syringe followed by ZnCl₂ (24 mg, 0.18 mmol) in MeOH (5 mL). The mixture was then stirred at room temperature overnight. The reaction mixture was then passed through a Celite plug, and the solvent in the filtrate was removed by rotary evaporation. The residue was deposited on a silica gel and purified by silica flash chromatography (2:3 AcOEt/hexanes with 5% Et₃N) to give Zn(Q-L2)₂ (0.10 g, 65%) as a crystalline blue solid. ¹H NMR (500 MHz, chloroform-d) δ 8.89 (dd, J = 4.3, 1.7 Hz, 4H), 8.40 (dt, J = 8.4, 1.3 Hz, 4H), 8.12 (dd, J = 7.5, 1.9 Hz, 8H), 8.06-8.00 (m, 4H), 7.71 (d, J = 7.8 Hz, 8H), 7.66-7.60 (m, 8H), 7.51 (d, J = 7.1 Hz, 12H), 7.27 (dd, J = 8.5, 4.2 Hz, 4H), 7.09 (d, J = 7.8 Hz, 8H), 2.46-2.36 (m, 8H), 1.41 (t, J = 7.8 Hz, 8Hz)Hz, 8H), 1.25-1.12 (m, 24H), 0.82 (t, J = 7.2 Hz, 12H). 13 C NMR (126 MHz, CDCl₃) δ 162.40, 150.75, 147.94, 146.51,

145.92, 145.54, 134.99, 133.19, 131.01, 130.05, 129.71, 129.65, 129.02, 128.42, 128.35, 128.28, 127.80, 127.76, 122.04, 121.35, 111.91, 93.89, 91.20, 77.27, 77.02, 76.77, 35.87, 31.63, 31.02, 29.35, 22.68, 14.14. MALDI-TOF-MS m/z: calcd. for $C_{132}H_{112}N_{10}Zn$, 1900.84; found, 1902.08. Anal. Calcd for C, 83.28; H, 5.93; N, 7.36; found: C, 82.90; H, 5.90; N, 7.32.

ASSOCIATED CONTENT

Solution Supporting Information

The Supporting Information is available free of charge at https://pubs.acs.org/doi/10.1021/acsomega.0c05169.

General characterization methods and instrumentation, NMR spectra, MALDI-TOF MS spectra, thermal properties, UV—vis spectra, crystal data, energy decomposition analysis, electrochemistry data, and transfer integrals (PDF)

Crystallographic data of Zn(Q-L2), (CIF)

AUTHOR INFORMATION

Corresponding Author

Genevieve Sauvé — Department of Chemistry, Case Western Reserve University, Cleveland, Ohio 44122, United States; orcid.org/0000-0002-9721-0447; Phone: 1-216-365-3668; Email: genevieve.sauve@case.edu

Authors

Chenwei Lu — Department of Chemistry, Case Western Reserve University, Cleveland, Ohio 44122, United States; orcid.org/0000-0002-5170-8979

Chunlai Wang — Department of Chemistry, Case Western Reserve University, Cleveland, Ohio 44122, United States; orcid.org/0000-0002-3519-4293

Jayvic C. Jimenez – Department of Chemistry, Case Western Reserve University, Cleveland, Ohio 44122, United States

Arnold L. Rheingold – Department of Chemistry and Biochemistry, University of California San Diego, La Jolla, California 92093, United States

Complete contact information is available at: https://pubs.acs.org/10.1021/acsomega.0c05169

Notes

The authors declare no competing financial interest. CCDC 2020028 contains the supplementary crystallographic data for this paper. These data can be obtained free of charge via www.ccdc.cam.ac.uk/data_request/cif, or by emailing data_request@ccdc.cam.ac.uk, or by contacting The Cambridge Crystallographic Data Centre, 12 Union Road, Cambridge CB2 1EZ, UK; fax: +44 1223 336033.

ACKNOWLEDGMENTS

We are grateful to the National Science Foundation (CHEM 1904868) for funding this project. This work was possible thanks to NSF MRI-0821515 for MALDI-TOF-TOF and NSF MRI-1334048 for NMR instrumentation.

REFERENCES

- (1) Handbook of Conducting Polymers; 3rd ed.; CRC Press: New York, 2007.
- (2) Newman, C. R.; Frisbie, C. D.; da Silva Filho, D. A.; Brédas, J.-L.; Ewbank, P. C.; Mann, K. R. Introduction to Organic Thin Film Transistors and Design of n-Channel Organic Semiconductors. *Chem. Mater.* **2004**, *16*, 4436–4451.

- (3) Sirringhaus, H. 25th anniversary article: organic field-effect transistors: the path beyond amorphous silicon. *Adv. Mater.* **2014**, *26*, 1319–1335.
- (4) Takimiya, K.; Nakano, M.; Sugino, H.; Osaka, I. Design and elaboration of organic molecules for high field-effect-mobility semiconductors. *Synth. Met.* **2016**, 217, 68–78.
- (5) Coropceanu, V.; Cornil, J.; da Silva Filho, D. A.; Olivier, Y.; Silbey, R.; Brédas, J. L. Charge transport in organic semiconductors. *Chem. Rev.* **2007**, *107*, 926–952.
- (6) Bredas, J. L.; Calbert, J. P.; da Silva Filho, D. A.; Cornil, J. Organic semiconductors: a theoretical characterization of the basic parameters governing charge transport. *Proc. Natl. Acad. Sci. U. S. A.* **2002**. *99*. 5804–5809.
- (7) Marcus, R. A. Electron transfer reactions in chemistry: theory and experiment (Nobel lecture). *Angew. Chem., Int. Ed. Engl.* **1993**, 32, 1111–1121.
- (8) Nelson, J. Polymer:fullerene bulk heterojunction solar cells. *Mater. Today* **2011**, *14*, 462–470.
- (9) Li, G.; Zhu, R.; Yang, Y. Polymer solar cells. *Nat. Photonics* **2012**, *6*, 153–161.
- (10) Lin, Y.; Zhan, X. Non-fullerene acceptors for organic photovoltaics: an emerging horizon. *Mater. Horiz.* **2014**, *1*, 470–488.
- (11) Rajaram, S.; Shivanna, R.; Kandappa, S. K.; Narayan, K. S. Nonplanar Perylene Diimides as Potential Alternatives to Fullerenes in Organic Solar Cells. *J. Phys. Chem. Lett.* **2012**, *3*, 2405–2408.
- (12) Dittmer, J. J.; Lazzaroni, R.; Leclère, P.; Moretti, P.; Granström, M.; Petritsch, K.; Marseglia, E. A.; Friend, R. H.; Brédas, J. L.; Rost, H.; Holmes, A. B. Crystal network formation in organic solar cells. *Sol. Energy Mater. Sol. Cells* **2000**, *61*, 53–61.
- (13) Sauvé, G.; Fernando, R. Beyond Fullerenes: Designing Alternative Molecular Electron Acceptors for Solution-Processable Bulk Heterojunction Organic Photovoltaics. *J. Phys. Chem. Lett.* **2015**, 6, 3770–3780.
- (14) Sauvé, G. Designing alternative non-fullerene molecular electron acceptors for solution-processable organic photovoltaics. *Chem. Rec.* **2019**, *19*, 1–1092.
- (15) Zhang, G.; Zhao, J.; Chow, P. C. Y.; Jiang, K.; Zhang, J.; Zhu, Z.; Zhang, J.; Huang, F.; Yan, H. Nonfullerene Acceptor Molecules for Bulk Heterojunction Organic Solar Cells. *Chem. Rev.* **2018**, *118*, 3447—3507.
- (16) Cheng, P.; Li, G.; Zhan, X.; Yang, Y. Next-generation organic photovoltaics based on non-fullerene acceptors. *Nat. Photonics* **2018**, *12*, 131–142.
- (17) Ge, Y.; O'Shea, D. F. Azadipyrromethenes: from traditional dye chemistry to leading edge applications. *Chem. Soc. Rev.* **2016**, *45*, 3846–3864.
- (18) Senevirathna, W.; Sauvé, G. Introducing 3D conjugated acceptors with intense red absorption: homoleptic metal(ii) complexes of di(phenylacetylene) azadipyrromethene. *J. Mater. Chem. C* **2013**, *1*, 6684–6694.
- (19) Mao, Z.; Senevirathna, W.; Liao, J. Y.; Gu, J.; Kesava, S. V.; Guo, C.; Gomez, E. D.; Sauvé, G. Azadipyrromethene-Based Zn(II) Complexes as Nonplanar Conjugated Electron Acceptors for Organic Photovoltaics. *Adv. Mater.* **2014**, *26*, 6290–6294.
- (20) Wang, C.; Wei, P.; Ngai, J. H. L.; Rheingold, A. L.; Gray, T. G.; Li, Y.; Pentzer, E.; Li, R.; Zhu, L.; Sauvé, G. A zinc(ii) complex of di(naphthylethynyl)azadipyrromethene with low synthetic complexity leads to OPV with high industrial accessibility. *J. Mater. Chem. A* **2019**, *7*, 24614–24625.
- (21) Wang, C.; Zhao, M.; Rheingold, A. L.; Sauvé, G. Structure—Property Study of Homoleptic Zinc(II) Complexes of Di(arylethynyl) Azadipyrromethene as Nonfullerene Acceptors for Organic Photovoltaics: Effect of the Aryl Group. *J. Phys. Chem. C* **2020**, 124, 8541–8549.
- (22) Po, R.; Bianchi, G.; Carbonera, C.; Pellegrino, A. "All That Glisters Is Not Gold": An Analysis of the Synthetic Complexity of Efficient Polymer Donors for Polymer Solar Cells. *Macromolecules* **2015**, *48*, 453–461.

- (23) Po, R.; Bernardi, A.; Calabrese, A.; Carbonera, C.; Corso, G.; Pellegrino, A. From lab to fab: how must the polymer solar cell materials design change? an industrial perspective. *Energy Environ. Sci.* **2014**, *7*, 925—943.
- (24) Li, N.; McCulloch, I.; Brabec, C. J. Analyzing the efficiency, stability and cost potential for fullerene-free organic photovoltaics in one figure of merit. *Energy Environ. Sci.* **2018**, *11*, 1355–1361.
- (25) Godard, A.; Jacquelin, J.-M.; Quéguiner, G. Etude de la metallation des pivalamido-2, -3 et -4 quinoleine. *J. Organomet. Chem.* **1988**, 354, 273–285.
- (26) Wendler, K.; Thar, J.; Zahn, S.; Kirchner, B. Estimating the Hydrogen Bond Energy. J. Phys. Chem. A 2010, 114, 9529-9536.
- (27) Su, P.; Li, H. Energy decomposition analysis of covalent bonds and intermolecular interactions. *J. Chem. Phys.* **2009**, *131*, No. 014102.
- (28) Steinmann, S. N.; Corminboeuf, C.; Wu, W.; Mo, Y. Dispersion-corrected energy decomposition analysis for intermolecular interactions based on the BLW and dDXDM methods. *J. Phys. Chem. A* **2011**, *115*, 5467–5477.
- (29) Stasyuk, O. A.; Sedlak, R.; Guerra, C. F.; Hobza, P. Comparison of the DFT-SAPT and Canonical EDA Schemes for the Energy Decomposition of Various Types of Noncovalent Interactions. *J. Chem. Theory Comput.* **2018**, *14*, 3440–3450.
- (30) Guillaumes, L.; Simon, S.; FonsecaGuerra, C. The Role of Aromaticity, Hybridization, Electrostatics, and Covalency in Resonance-Assisted Hydrogen Bonds of Adenine-Thymine (AT) Base Pairs and Their Mimics. *ChemistryOpen* **2015**, *4*, 318–327.
- (31) Fonseca Guerra, C.; van der Wijst, T.; Poater, J.; Swart, M.; Bickelhaupt, F. M. Adenine versus guanine quartets in aqueous solution: dispersion-corrected DFT study on the differences in π -stacking and hydrogen-bonding behavior. *Theor. Chem. Acc.* **2009**, 125, 245–252.
- (32) te Velde, G.; Bickelhaupt, F. M.; Baerends, E. J.; Fonseca Guerra, C.; van Gisbergen, S. J. A.; Snijders, J. G.; Ziegler, T. Chemistry with ADF. J. Comput. Chem. 2001, 22, 931–967.
- (33) ADF 2019.3, SCM, Theoretical Chemistry; Vrije Universiteit, Amsterdam, The Netherlands, http://www.scm.com.
- (34) Bickelhaupt, F. M.; Baerends, E. J. Khon-Sham Density Functional Theory: Predicting and Understanding Chemistry. In *Rev. Comput. Chem.*; Lipkowitz, K. B.; Boyd, D. B., Eds. Wiley-VCH: New York, 2000; Vol. 15, pp. 1–86.
- (35) Jeffrey, G. A. An introduction to hydrogen bonding; Oxford University Press: New York, 1997; p 320.
- (36) van der Lubbe, S. C. C.; Fonseca Guerra, C. Hydrogen-Bond Strength of CC and GG Pairs Determined by Steric Repulsion: Electrostatics and Charge Transfer Overruled. *Chemistry* **2017**, 23, 10249–10253.
- (37) Fonseca Guerra, C.; Bickelhaupt, F. M.; Snijders, J. G.; Baerends, E. J. The Nature of the Hydrogen Bond in DNA Base Pairs: The Role of Charge Transfer and Resonance Assistance. *Chem. Eur. J.* 1999, *5*, 3581–3594.
- (38) Seldenthuis, J. S. Electrical and mechanical effects in single-molecule junctions. PhD, Delft University of Technology, 2011.
- (39) Verzijl, C. J. O.; Seldenthuis, J. S.; Thijssen, J. M. Applicability of the wide-band limit in DFT-based molecular transport calculations. *J. Chem. Phys.* **2013**, *138*, No. 094102.
- (40) Deng, W.-Q.; Sun, L.; Huang, J.-D.; Chai, S.; Wen, S.-H.; Han, K.-L. Quantitative prediction of charge mobilities of π -stacked systems by first-principles simulation. *Nat. Protoc.* **2015**, *10*, 632–642.